Nano Research 2015, 8(8): 2744–2754
DOI 10.1007/s12274-015-0781-3
Research Article
ISSN 1998-0124
CN 11-5974/O4

Facile electrodeposition of 3D concentration-gradient Ni–Co hydroxide nanostructures on nickel foam as high performance electrodes for asymmetric supercapacitors

Mingyang Yang[1,2], Hua Cheng[1], Yingying Gu[2], Zhifang Sun[1], Jing Hu[1], Lujie Cao[1], Fucong Lv[1], Minchan Li[1,2], Wenxi Wang[1], Zhenyu Wang[1,2], Shaofei Wu[1], Hongtao Liu[2], and Zhouguang Lu[1] (✉)

[1] *Department of Materials Science and Engineering, South University of Science and Technology of China, Shenzhen 518055, China*
[2] *College of Chemistry and Chemical Engineering, Central South University, Changsha 410083, China*

Received: 2 December 2014
Revised: 2 April 2015
Accepted: 5 April 2015

KEYWORDS
electrodeposition, concentration-gradient, nickel cobalt hydroxides, supercapacitors

ABSTRACT

Novel three-dimensional (3D) concentration-gradient Ni–Co hydroxide nanostructures (3DCGNC) have been directly grown on nickel foam by a facile stepwise electrochemical deposition method and intensively investigated as binder- and conductor-free electrode for supercapacitors. Based on a three-electrode electrochemical characterization technique, the obtained 3DCGNC electrodes demonstrated a high specific capacitance of 1,760 $F \cdot g^{-1}$ and a remarkable rate capability whereby more than 62.5% capacitance was retained when the current density was raised from 1 to 100 $A \cdot g^{-1}$. More importantly, asymmetric supercapacitors were assembled by using the obtained 3DCGNC as the cathode and Ketjenblack as a conventional activated carbon anode. The fabricated asymmetric supercapacitors exhibited very promising electrochemical performances with an excellent combination of high energy density of 103.0 $Wh \cdot kg^{-1}$ at a power density of 3.0 $kW \cdot kg^{-1}$, and excellent rate capability—energy densities of about 70.4 and 26.0 $Wh \cdot kg^{-1}$ were achieved when the average power densities were increased to 26.2 and 133.4 $kW \cdot kg^{-1}$, respectively. Moreover, an extremely stable cycling life with only 2.7% capacitance loss after 20,000 cycles at a current density of 5 $A \cdot g^{-1}$ was achieved, which compares very well with the traditional double-layer supercapacitors.

1 Introduction

Supercapacitors have attracted increasing research interest as energy storage devices by virtue of their low cost, being environmentally friendly, long lifespan, and—in particular—their prominent power capability [1]. According to the charge storage mechanism, supercapacitors are categorized into two classes: electrochemical double layer capacitors (EDLCs) where electric charge is stored in a capacitor through

Address correspondence to luzg@sustc.edu.cn

charge separation at the electrode–electrolyte interface without any electron transfer; and pseudocapacitors governed by reversible redox and/or electro-sorption/desorption reactions occurring at the surface of electroactive materials. EDLCs based on activated carbon have been successfully commercialized and have the advantages of excellent power capability and long-term cycling stability. However these EDLCs exhibit very limited energy density which has hindered their wide application in electric vehicles (EVs) [2]. Pseudocapacitors based on transition metal oxides, such as RuO_2, Mn_3O_4, SnO_2, V_2O_5, Fe_3O_4, NiO/$Ni(OH)_2$, Co_3O_4/$Co(OH)_2$ and $NiCo_2O_4$, exhibit much higher energy density compared with EDLCs but at the expense of reduced power density and lower service durability [3–12]. When pseudocapacitive electrodes are coupled with electrical double-layer capacitive carbon materials to construct asymmetric supercapacitors, a good combination of high energy and power density as well as stable cycling performance can be achieved [13–15]. However, the relatively slow ion diffusion rates, poor electron conductivity and volume variation of pseudocapacitive materials upon electrochemical reaction remain critical issues which significantly inhibit their practical applications for EVs.

Recently, binder-free supercapacitive electrodes directly grown on three-dimensional conductive substrates such as nickel foams, carbon nanotube arrays or porous metallic films have attracted great attention because this process can enhance the effective contact area between active materials and electrolytes as well as reinforce the interfacial contact between the current collector and active materials and thus considerably improve the ion and electron transport, leading to much improved electrochemical activities. For instance, $NiCo_2O_4$, $NiFe_2O_4$ and $ZnCo_2O_4$ have been directly grown on various conductive substrates—including carbon fiber paper, carbon cloth, and nickel foam–and shown to have excellent electrochemical performances [16–18].

Nanostructured nickel and cobalt hydroxides have been intensively studied as pseudocapacitive materials by virtue of their high theoretical specific capacitances (2,365 $F \cdot g^{-1}$ for $Ni(OH)_2$ and 3,560 $F \cdot g^{-1}$ for $Co(OH)_2$), good cyclic stability, and environmental friendliness [19, 20]. However, $Ni(OH)_2$ has slow ion diffusion rates and poor electrical conductivity resulting in poor cycling life and moderate charge–discharge rates. For instance, Li et al. electrodeposited $Ni(OH)_2$ on nickel foams which showed a very high specific capacitance of 3,152 $F \cdot g^{-1}$, but poor cycling stability (a significant capacitance loss of about 48% of the initial capacitance was observed after only 300 cycles) [21]. The substitution of Ni by Co to form Ni–Co double hydroxides can effectively reduce the resistance of the electrode and raise the oxygen over-potential. The Co component also participates in the electrochemical redox reaction without reducing the specific capacitance [22, 23]. Wu et al. presented a one-step method for growing Ni–Co layered double hydroxide hybrid films on nickel foam with ultrathin nanosheets and porous nanostructures and, when used in supercapacitors, showed a high specific capacitance of 2,682 $F \cdot g^{-1}$ at 3 $A \cdot g^{-1}$—a value that is much higher than those for the single component counterparts. Further, an asymmetric supercapacitor was fabricated by using reduced graphene oxide as the counter electrode and an ultrahigh energy density of 188 $Wh \cdot kg^{-1}$ was achieved at an average power density of 1,499 $W \cdot kg^{-1}$. However, the energy density rapidly decreased to 21.8 $Wh \cdot kg^{-1}$ when the power density was increased to 7,324 $W \cdot kg^{-1}$ [24]. It has been found that electrodeposited unitary $Co(OH)_2$ on nickel foam gave high rate performance and good cycle stability, but the observed specific capacitance (1,310 $F \cdot g^{-1}$ at 1 $A \cdot g^{-1}$) was much lower than its theoretical specific capacitance [25].

In this paper, we present a facile stepwise electrochemical deposition method to directly synthesize three-dimensional (3D) concentration-gradient Ni–Co hydroxide nanostructures (denoted 3DCGNC) on nickel foam for use in supercapacitors, as schematically illustrated in Fig. 1. The Ni–Co double hydroxide nanosheets with different Ni/Co ratios of 1/0, 2/1, 1/1, 1/2 and 0/1 were successively electrodeposited on the nickel foams in turn to form the 3D concentration-gradient nanostructure. During the deposition, a very interesting phenomenon was observed whereby the newly growing nanosheets were inserted in the pores of the previously grown layer to form nearly continuous concentration-gradient hierarchical nanostructures which can provide high specific surface area and

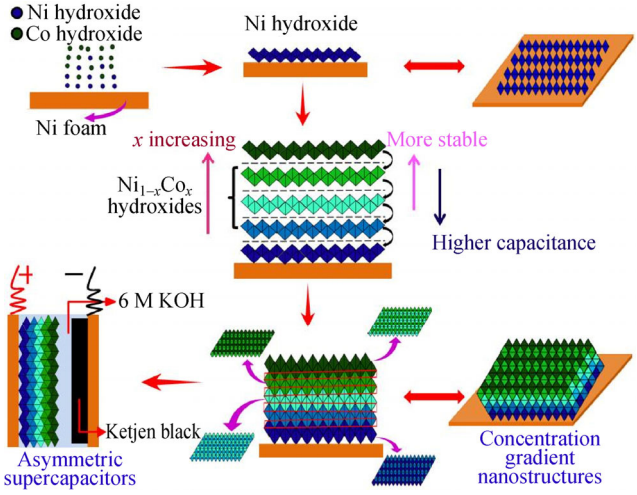

Figure 1 Schematic illustration of the formation mechanism of 3DCGNC directly grown on Ni foams by a step-wise electrochemical deposition method and the assembly of asymmetric supercapacitors based on the as-obtained 3DCGNC.

a stable scaffold leading to considerably enhanced electrochemical activities. Several advantages can be expected from this novel 3D concentration-gradient nanostructure: (i) The 3DCGNC directly grown on the three-dimensional nickel foam surfaces allow the easy access of electrolyte to the entire active materials and prevent any decrease in electrical conductivity caused by the electrical resistance of the binder; (ii) the multiphasic structure can avoid the aggregation of the different phases and keep the structure of 3DCGNC intact; (iii) the insertion of nanosheets between the different layers prevents the aggregation of a single phase; (iv) the Ni-rich inner layers ensure high capacitance and the Co-rich outer layers—which have good electron transportation properties—play a role of cladding and greatly enhance the cycling stability and the rate performance of the 3DCGNC. The as-obtained 3DCGNC electrode was used as a positive electrode in combination with the traditional Ketjenblack as a traditional activated carbon negative electrode to fabricate asymmetric supercapacitors (Fig. 1).

2 Experimental

2.1 Fabrication of the 3DCGNC and the Ni–Co hydroxides with constant Ni/Co compositions on nickel foams

All the chemicals used were of analytical grade and used without further purification. Nickel nitrate hexahydrate ($Ni(NO_3)_2{\cdot}6H_2O$), cobalt nitrate hexahydrate ($Co(NO_3)_2{\cdot}6H_2O$), hydrochloric acid (HCl), potassium hydroxide (KOH) and absolute ethanol were purchased from Sinopharm Chemical Reagent Co., Ltd. and Ketjenblack (EC-300J) from Mitsubishi Chemical, Japan. Deionized water was used. The electrochemical deposition of concentration-gradient Ni–Co hydroxide was carried out in a three-electrode cell at a constant current of –0.5 $mA{\cdot}cm^{-2}$. The working electrode was a piece of nickel foam (1 cm × 1 cm) which was treated with 3 M HCl for 10 min to remove the surface oxide layer and then washed thoroughly with deionized water before the electrodeposition. A Pt plate and a saturated calomel electrode (SCE) were used as the counter and reference electrode, respectively. The 3DCGNC was fabricated by successive electrodeposition procedure in 0.01 $mol{\cdot}L^{-1}$ metal ion solution with different Ni/Co concentration ratios of 1/0, 2/1, 1/1, 1/2 and 0/1. The electrodeposition time in each step during the constant current deposition was fixed at 120 s and the active material mass was controlled within 0.23 ± 0.02 $mg{\cdot}cm^{-2}$ (determined by weighing the nickel foam before and after the electrodeposition). For the sake of comparison, homogeneous composition Ni–Co hydroxide nanostructures with constant Ni/Co ratios of 1/0, 2/1, 1/1, 1/2 and 0/1 were also electrodeposited on Ni foam substrates by the same electrochemical procedure (with a constant current of –0.5 $mA{\cdot}cm^{-2}$ and duration of 600 s). The Ketjenblack electrode was prepared by pressing a mixture of 70 wt.% Ketjenblack and 30 wt.% polytetrafluoroethylene (PTFE) onto the nickel foam. The mass loading of the Ketjenblack electrode was approximately 0.75 ± 0.02 mg.

2.2 Materials characterization

X-ray diffraction (XRD) data were collected using a Rigaku D/MAX 2400 diffractometer (Japan) with Cu Kα radiation (λ = 1.5418 Å) operating at 40.0 kV, 60.0 mA. Field emission scanning electron microscopy (FESEM) measurements were conducted on a Hitachi S-4800 scanning electron microscope. High resolution transmission electron microscopy (HRTEM) image and energy dispersive X-ray spectroscopy (EDX)

measurements were obtained on a transmission electron microscope (FEI Tecnai G2 F30) equipped with an energy dispersive X-ray analysis system. X-ray photoelectron spectroscopy (XPS, ESCALAB 250Xi, Thermo Scientific) measurements were conducted to investigate the valence state and composition of Ni and Co in the concentration-gradient electrodes.

2.3 Electrochemical characterization

Electrochemical performance was evaluated by using a three-electrode configuration and employing 6 M KOH as electrolyte, a Pt plate as the counter electrode, and Hg/HgO as the reference electrode. Cyclic voltammetry (CV) was performed on a CHI660E electrochemical workstation (Chenhua, Shanghai). The galvanostatic charge–discharge data were collected on a NEWARE (CT-4008) cycler. 3DCGNC was used as the positive electrode material and Ketjenblack as the negative electrode material to fabricate the asymmetric supercapacitors. The electrochemical performance of Ketjenblack was investigated in a three-electrode system and that of the asymmetric supercapacitor was investigated in a two-electrode system on a CHI660E electrochemical workstation (Chenhua, Shanghai). CV measurements were carried out at different scanning rates between –1 and 0 V for the Ketjenblack, and between 0 and 1.5 V for the asymmetric supercapacitor. The capacitance (C) of the 3DCGNC electrode and Ketjenblack electrode were calculated from the galvanostatic charge–discharge curves as follows: $C = I \times \Delta t/(V \times m)$, where C (F·g^{-1}) is the specific capacitance, I (A) is the discharge current, Δt (s) is the discharge time, V (V) is the potential change during the discharge, and m (g) is the mass of the active material in the electrode. The C of the asymmetric supercapacitor was calculated from the galvanostatic charge–discharge curves as follows: $C = 4I \times \Delta t/(V \times m')$, where m'(g) is the total mass of the active material in the positive and negative electrodes. The energy and power densities of the obtained 3DCGNC- and Ketjenblack-based electrodes, and of the asymmetric supercapacitor were calculated as follows: $E = 0.5 \times C \times V^2$, $P_{ave} = E/\Delta t$, where E (Wh·kg^{-1}) is the energy density, V(V) is the cell voltage excluding IR drop, P_{ave} (W·kg^{-1}) is the average power density, and t (s) is the discharge time [26, 27].

3 Results and discussion

3.1 Fabrication of the 3DCGNC

Figure 2(a) shows the XRD patterns of the obtained 3DCGNC, $Co(OH)_2$ and $Ni(OH)_2$. All the patterns consist of three sharp peaks due to the nickel foam substrate. In the XRD pattern of the 3DCGNC, there are four additional weak peaks appearing at the 2θ values of 11.4° (7.75 Å), 22.8° (3.91 Å), 34.0° (2.68 Å) and 59.6° (1.55 Å), that can be indexed to the (003), (006), (012), and (110) reflections of α-$Co(OH)_2$ or α-$Ni(OH)_2$ [23, 25, 28]. It was difficult to differentiate between the two phases of α-$Co(OH)_2$ and α-$Ni(OH)_2$ from the XRD pattern, since they have very similar crystal structures, and their diffraction spectra are almost identical. However, there are no obvious peaks observed at 11.4° and 22.8° in the XRD pattern for $Ni(OH)_2$ indicating it has low crystallinity. In order to investigate the composition variation along the film, we purposely prepared Ni–Co hydroxide nanostructures on polished flat nickel plates by the same step-wise electrochemical deposition process. Depth profile XPS as employed to analyse the elemental distribution of the 3DCGNC electrode along the direction perpendicular to the substrate as shown in Fig. 2(b). The sample was etched at a rate of 12 nm·min^{-1} by Ar^+ ions. In this figure only the spectra taken after every 60 nm etching were shown. The two obvious shakeup satellites (indicated as "Sat") close to two spin-orbit doublets at 873.3 and 855.6 eV can be identified as Ni $2p_{1/2}$ and Ni $2p_{3/2}$ signals of Ni^{2+}, respectively [29]. In the Co 2p XPS profiles, the spin- orbit splitting value of Co $2p_{1/2}$ and Co $2p_{3/2}$ is 15.2 eV, and the Co $2p_{3/2}$ satellite line intensity is pretty low, suggesting the co-existence of Co^{2+} and Co^{3+} in the hybrid nanosheets [30, 31]. These results indicate that the as-obtained hybrid nanosheets are actually Ni–Co layered double hydroxides (LDHs). In addition, we can also see that the intensity of Co becomes weaker and the intensity of Ni is enhanced with increasing etching depth. Surprisingly, although only $Ni(NO_3)_2$ and $Co(NO_3)_2$ were respectively used in the electrodeposition electrolyte for the first layer attached to the substrate and for the final layer on top of the film surface, both Co and Ni components were detected in these two layers. The atomic compositions

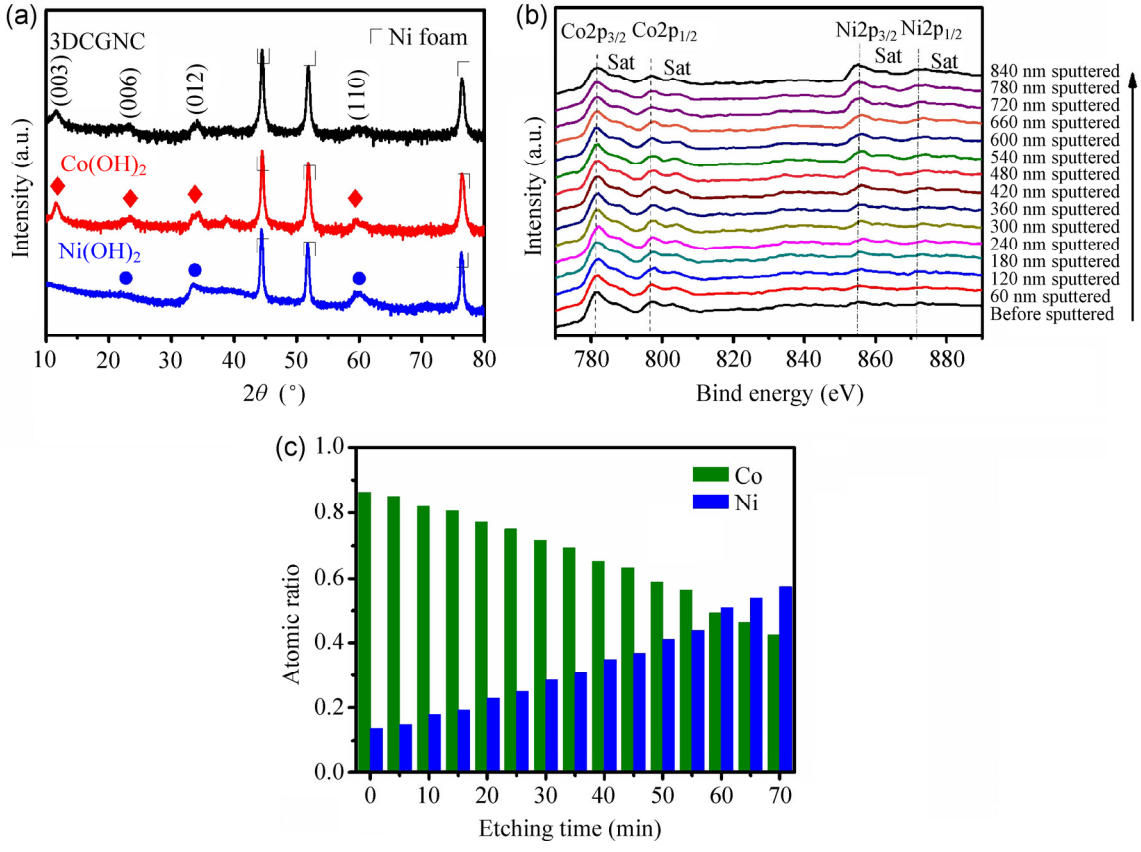

Figure 2 (a) XRD pattern of the 3DCGNC (black line), $Co(OH)_2$ (red line) and $Ni(OH)_2$ (blue line). (b) Depth profile XPS of the electrode. The arrow indicates the increase of surface sputtering depth. The histogram in (c) summarizes the variation in the relative composition of Co and Ni as a function of the surface etching time. The samples for XPS analysis were grown on a flat Ni plate by an identical step-wise electrochemical deposition method to that used for fabricating the 3DCGNC electrodes.

of Co and Ni as a function of etching time deduced from the XPS were calculated and the results are shown in Fig. 2(c). The Co content decreases and the Ni content increases gradually on going from the surface to the substrate. The actual composition distribution of the obtained film was not consistent with the feeding ratio of Ni/Co in the electrodeposition electrolyte.

The FESEM images in Fig. 3 show the surface morphology of the concentration-gradient nanostructures on nickel foam after the deposition of different layers. Figure 3(a) displays the $Ni(OH)_2$ layer electrodeposited first onto the nickel foam surface. The $Ni(OH)_2$ coating contains very small grains (about 10 nm in diameter) forming a 3D and mesoporous structure [21]. From Fig. 3(b), we can see that the morphology of the second layer electrodeposited on the first layer of $Ni(OH)_2$ is quite different from the first layer and shows a honeycomb-like nanostructure with macroporosity, with a pore diameter of about 100 nm. The third (c), fourth (d) and fifth (e) layers have similar pore diameters of approximately 50 nm. This value is much smaller than the pore diameter of the different films electrodeposited on nickel foam by using constant Ni/Co compositions of 1/1, 1/2 and 0/1 which have pore diameters of above 100 nm (see Fig. S2 in the Electronic Supplementary Material (ESM)). We presume that the growth of the new layers starts from the pores of the previous layer. In order to clearly study the cross-section composition distribution and morphology, 3D nickel foam was replaced with flat Ni plate as a substrate on which similar concentration-gradient $Ni_xCo_{1-x}(OH)_2$ nanostructures were deposited. The cross-section SEM images and the corresponding composition distribution spectra are shown in Fig. 3(f). These show that the

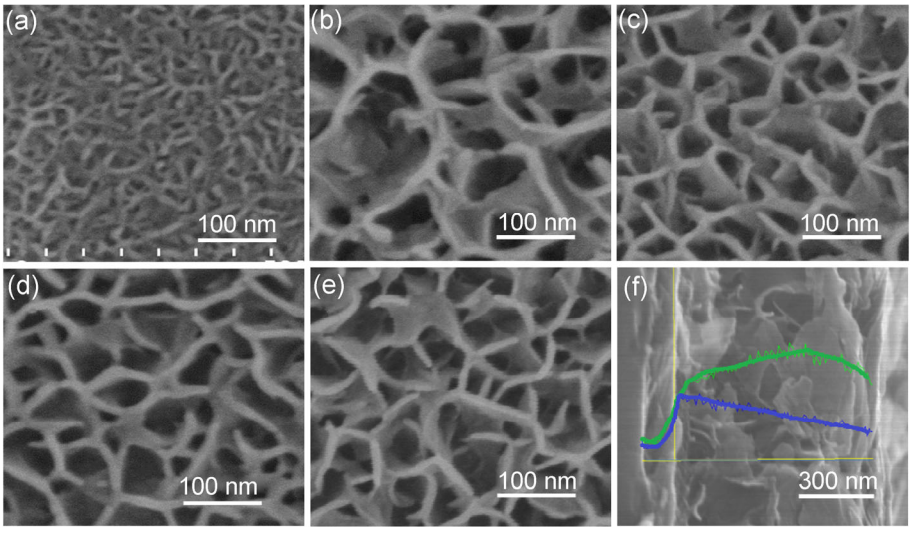

Figure 3 SEM images showing the surface of the concentration-gradient Ni–Co hydroxide nanostructures after the completion of (a) the first (Ni/Co = 1/0), (b) the second (Ni/Co = 2/1), (c) the third (Ni/Co = 1/1), (d) the fourth (Ni/Co = 1/2), and (e) the fifth layer (Ni/Co = 0/1) deposition. (f) Cross-section SEM image of the 3DCGNC deposited on a flat Ni plate. The inset in (f) shows the Ni (blue) and Co (green) EDS composition distribution of this electrode.

content of Ni decreases and the fraction of Co increases on going from the Ni substrate to the film surface. As a result, the Ni/Co composition keeps changing gradually along the cross-section. The thickness is approximately 900 nm, which is in accordance with the previous XPS results.

We suggest that during the formation of 3DCGNC, each deposition layer grows onto the previous deposition layer and the newly growing nanosheets are preferentially inserted into the pores located a short distance from the substrate which provide a low resistance. The insertion of the different layers which have different compositions leads to a nearly continuous concentration variation from the substrate to the surface of the obtained 3DCGNC. Therefore, we have successfully synthesized 3D concentration-gradient Ni–Co hydroxide nanostructures on the nickel foam by a facile step-wise electrochemical deposition method by using five different compositions of electrolytes.

3.2 Electrochemical performance of 3DCGNC

In order to investigate the electrochemical performance of the 3DCGNC-electrode, we first recorded the CV curves of the Ni–Co hydroxide electrodes electrodeposited on Ni foam with constant Ni/Co compositions for the purposes of comparison. All the electrodes were tested in 6 M KOH solutions. As shown in Fig. S4 (in the ESM), a pair of peaks appears in the curve for $Ni(OH)_2$ between 0.25 and 0.5 V arising from the pseudocapacitive reaction of Ni^{2+}/Ni^{3+}, and two pairs of peaks in the unitary $Co(OH)_2$ between –0.1 and 0.5 V arising from the redox reactions of Co^{2+}/Co^{3+} and Co^{3+}/Co^{4+}. All the Ni–Co LDH electrodes show two pairs of redox peaks, with the peaks at lower potential left-shifted with increasing Co content because of the synergetic effect of different Ni/Co ratios [25, 32]. Among all the samples, the Ni–Co LDH electrode with a Ni/Co mole ratio of 2/1 demonstrates the largest peak area, indicating this material has the highest specific capacitance among all the electrodes. Figure 4(a) shows the CV curves of the 3DCGNC. There are three pairs of peaks at low scan rates in the potential between 0 and 0.5 V, which indicates that the 3DCGNC-electrode has much better pseudocapacitive activities than the LDH materials, because of the interactions between the different components. The 3DCGNC electrode has only two pairs of redox peaks in the CV curves recorded at higher scan rates because the redox reactions are not very obvious when the electrode is charged/discharged too fast. Figure 4(b) shows the galvanostatic discharge curves of the 3DCGNC electrode for different current densities. The voltage gradually decreases as discharging proceeds,

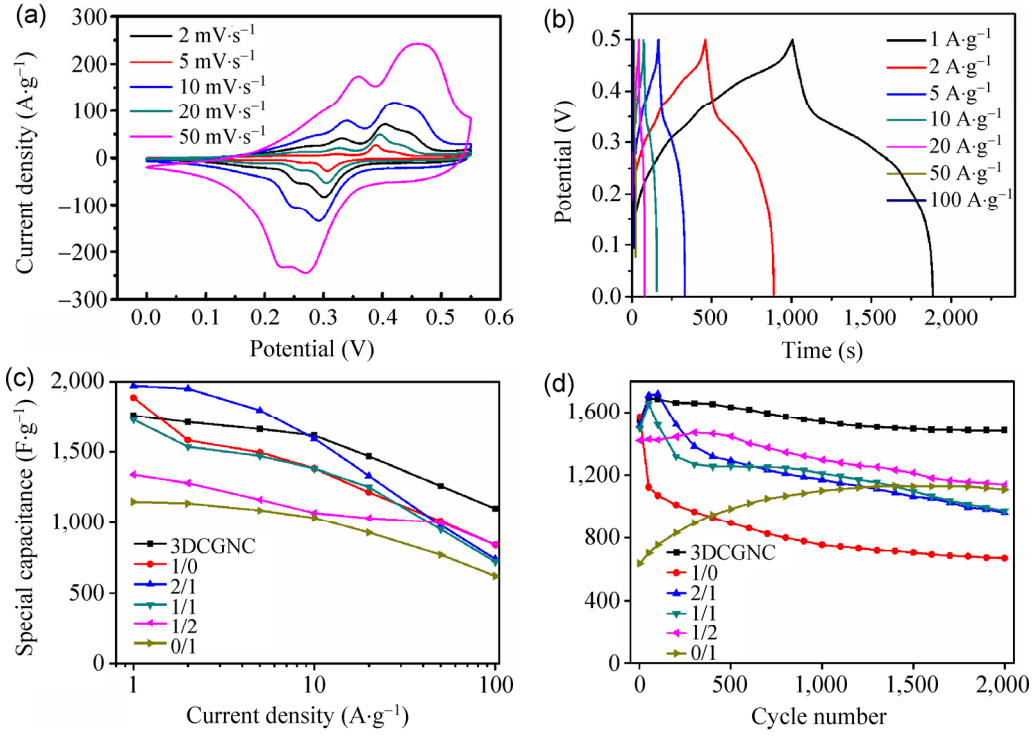

Figure 4 (a) CV curves of the 3DCGNC electrode at different scan rates. (b) Galvanostatic charge and discharge curves of the 3DCGNC electrode at different current densities. Comparison of (c) rate performance and (d) cycling performance of the 3DCGNC and Ni–Co LDH hybrid electrodes prepared with different Ni/Co feeding molar ratios. The testing was performed based on three-electrode configurations.

characteristic of typical pseudocapacitive behavior. The specific capacitances were calculated to be 1,760, 1,712, 1,662, 1,616, 1,468, 1,260, and 1,100 F·g^{-1} at current densities of 1, 2, 5, 10, 20, 50, and 100 A·g^{-1}, respectively. Figure 4(c) shows the specific capacitance as a function of current density, and the cycling performance of the 3DCGNC and the Ni–Co LDH-electrodes with constant Ni/Co compositions measured at a current density of 10 A·g^{-1} are shown in Fig. 4(d). We further summarize the electrochemical properties of the 3DCGNC electrode and the Ni–Co LDH electrodes with different compositions in Table 1. The Ni–Co LDH electrodes with Ni/Co mole ratios of 1/0, 2/1 and 1/1 exhibit capacitances of 1,888, 1,971 and 1,720 F·g^{-1}, respectively, at the low current density of 1 A·g^{-1}. However, the Ni-rich LDH electrodes have poor electronic conductivity leading to poor rate performance when the current density was increased from 1 to 100 A·g^{-1}. After 2,000 cycles at 10 A·g^{-1}, the capacitance retention of the 1/0, 2/1 and 1/1 Ni–Co LDH electrodes are only 42.5%, 55.3% and 58.7%, respectively. The 1/2 and 0/1 Ni–Co LDH electrodes with the higher Co contents have much better rate performance which can be attributed to the excellent electronic conductivity of $Co(OH)_2$. However they exhibited relatively lower specific capacitance of only 1,342 and 1,149 F·g^{-1}, respectively, at 1 A·g^{-1}. As for the 3DCGNC electrode, the reversible specific capacitance

Table 1 Comparison of the electrochemical performance of the Ni–Co LDH electrodes with different Ni/Co ratios and the 3DCGNC-electrode

Ni–Co LDH electrode	Capacitance (1 A·g^{-1})	Rate performance (100 A·g^{-1} vs. 1 A·g^{-1})	Capacitance retention after 2,000 cycles
1/0	1,888 F·g^{-1}	45.5%	42.5%
2/1	1,971 F·g^{-1}	37.5%	55.3%
1/1	1,720 F·g^{-1}	42.1%	58.7%
1/2	1,342 F·g^{-1}	62.5%	79.3%
0/1	1,149 F·g^{-1}	52.5%	97.9%
3DCGNC	1,760 F·g^{-1}	62.5%	87.3%

of 1,760 $F \cdot g^{-1}$ is much higher than the values for the two LDH electrodes. Moreover, the 3DCGNC electrode demonstrates superior rate performance and excellent cycle performance, with a capacitance retention of 87.3% after 2,000 cycles. Overall, the 3DCGNC electrode exhibits superior electrochemical performance with a good combination of high specific capacitance, excellent rate performance and extremely stable cycle-life. The excellent electrochemical properties of the 3DCGNC electrode can be attributed to synergetic effects in the very special and novel concentration-gradient nanostructures: (a) The Ni-rich inner layers provide high specific capacitance and the Co-rich outer layers ensure high rate performance and long cycle life because $Co(OH)_2$ possesses high electronic conductivity; (b) the unique concentration-gradient nanostructure of the 3DCGNC prevents aggregation and collapse of the electrode leading to improved cycling stability.

3.3 Electrochemical performance of the asymmetric supercapacitors

To achieve higher energy density and power density, the 3DCGNC was used as the positive electrode and Ketjenblack used as the negative electrode to fabricate an asymmetric supercapacitor. Firstly, the electrochemical properties of the Ketjenblack were tested in the three-electrode configuration and the results are shown in Fig. S6 (in the ESM). The well-defined rectangular CV curves indicate excellent electrical double-layer capacitance properties at –1.0 to 0.0 V. Based on the galvanostatic charge–discharge curves as shown in Fig. S7 (in the ESM), the specific capacitance of the Ketjenblack was calculated to be 165.3, 125.6, 110.5, and 105 $F \cdot g^{-1}$ at current densities of 1, 2, 5 and 10 $A \cdot g^{-1}$, respectively.

Figure 5(a) shows the CV curves of the 3DCGNC and Ketjenblack separately in the three-electrode configuration, which demonstrate the good matching of these two electrodes for assembling asymmetric supercapacitors. Based on this, we fabricated an asymmetric supercapacitor by using the 3DCGNC as the positive electrode and Ketjenblack as the negative electrode. The CV curves of the asymmetric supercapacitors shown in Fig. 5(b) exhibit contributions from both electrical double-layer capacitance and pseudocapacitance in the potential range of 0–1.5 V. Galvanostatic charge–discharge curves for different current densities are shown in Fig. 5(c). Almost linear plots were observed, indicating the low internal resistance and excellent rate performance of the as-fabricated asymmetric supercapacitor. The specific capacitance of the asymmetric supercapacitor was calculated based on the total mass of anode and cathode. A high specific capacitance of 332 $F \cdot g^{-1}$ was obtained at 1 $A \cdot g^{-1}$, and a value as high as 187 $F \cdot g^{-1}$ was retained when the current density was increased significantly to 100 $A \cdot g^{-1}$, suggesting excellent rate performance. From Fig. 5(d), we can see the rate performance of the asymmetric supercapacitor is lower than that of 3DCGNC but higher than that of Ketjenblack, which indicates that the 3DCGNC has a pivotal influence in enhancing the rate performance of the asymmetric supercapacitors. Figure 5(e) compares the Ragone plots of 3DCGNC, Ketjenblack and the asymmetric supercapacitor, and clearly indicates the superior power density of the asymmetric supercapacitor as compared with the traditional Ketjenblack and the 3DCGNC. The energy densities of the asymmetric supercapacitor were calculated to be 103.0, 92.0, 76.6, 70.4, 63.5, 48.0 and 26.0 $Wh \cdot kg^{-1}$ at the average power densities of 3.0, 6.0, 9.5, 26.2, 50.8, 107.5 and 133.4 $kW \cdot kg^{-1}$, respectively. Therefore both high energy densities as well as high power densities can be achieved with this asymmetric supercapacitor. Figure 5(f) shows the cycling performance of the asymmetric supercapacitor. A capacitance loss of only 2.7% was found after 20,000 cycles, which compares favorably to traditional activated carbon-based electrical double layer supercapacitors. The inset of Fig. 5(f) shows the galvanostatic charge–discharge curves of this asymmetric supercapacitor, which exhibit linear and symmetric profiles, indicating excellent double-layer capacitive characteristics, which contribute to the extremely stable cycling performance of the as-obtained asymmetric supercapacitor. As a result, a desirable combination of high energy density, remarkable power density and extremely stable cycling performance was realized for the asymmetric supercapacitor based on the assembly of 3D concentration-gradient Ni–Co hydroxide nanostructures directly electrodeposited on nickel foam.

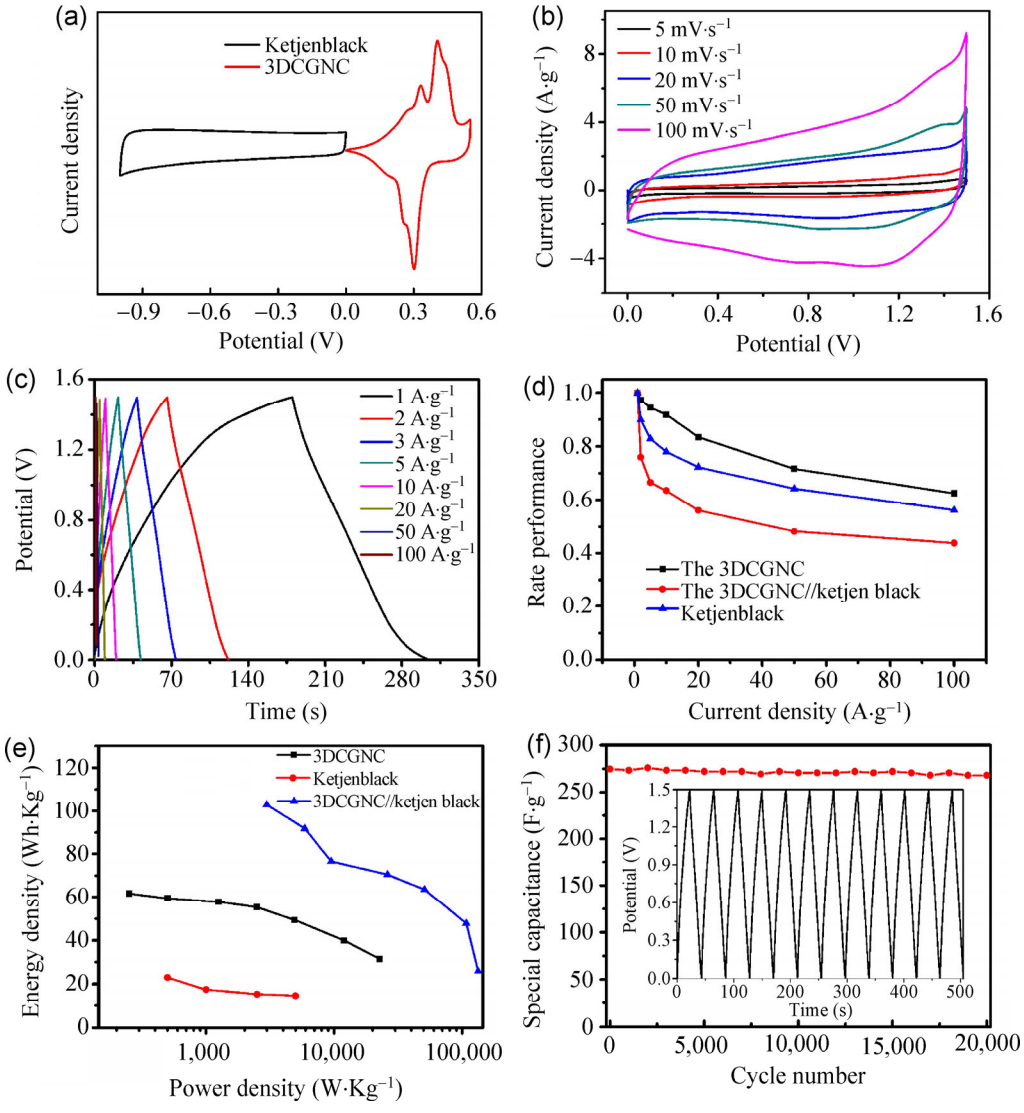

Figure 5 (a) CV curves of the 3DCGNC and Ketjenblack in different scanning voltage ranges based on three-electrode configurations. (b) CV curves at different scan rates and (c) galvanostatic charge and discharge curves at different current densities for the asymmetric supercapacitor assembled from a 3DCGNC cathode and a Ketjenblack anode. (d) Comparison of the rate performances of the single 3DCGNC electrode, the Ketjenblack electrode, and the asymmetric supercapacitor. The rate performance was normalized to the respective capacitance at a current density of 1 $A \cdot g^{-1}$. (e) Ragone plots showing the energy density as a function of power density for 3DCGNC, Ketjenblack and the asymmetric supercapacitor. (f) Cycling performance of the asymmetric supercapacitor at a current density of 5 $A \cdot g^{-1}$. The inset in (f) shows the galvanostatic charge–discharge curves of the asymmetric supercapacitor.

4 Conclusions

A novel 3DCGNC electrode with high capacitance, high rate performance and long-term stability has been synthesized by a simple stepwise electrochemical deposition method. When the 3DCGNC was used as the positive electrode paired with Ketjenblack as the negative electrode to fabricate an asymmetric supercapacitor, a high energy density of 103.0 $Wh \cdot kg^{-1}$ at a power density of 3.0 $kW \cdot kg^{-1}$ was obtained, together with excellent rate capability (with energy densities of about 70.4 and 26.0 $Wh \cdot kg^{-1}$ when the average power densities were increased to 26.2 and 133.4 $kW \cdot kg^{-1}$, respectively). Furthermore, this asymmetric supercapacitor exhibited extremely stable cycling performance with only 2.7% capacitance loss after 20,000 cycles, which is comparable to current commercial electrical double-layer supercapacitors. This facile strategy for the

direct synthesis of binder- and conductive additive-free electrodes possessing concentration-gradient hierarchical nanostructures offers new perspectives on the fabrication of a wide range of high performance electrode materials for use in next-generation supercapacitors and other energy storage devices.

Acknowledgements

This work was supported by the National Natural Science Foundation of China (No. 21001117), the Shenzhen Peacock Plan (No. KQCX20140522150815065), and the Starting-Up Funds of South University of Science and Technology of China (SUSTC) through the Talent Plan of the Shenzhen Government. H. T. L. acknowledges the support from a Key Project of the Hunan Provincial Science and Technology Plan (No. 2014FJ2007).

Electronic Supplementary Material: Supplementary material (details of EDS composition analysis, surface SEM images, TEM images, CV curves, and galvanostatic charge–discharge curves of the Ni–Co hydroxide samples with constant Ni/Co composition distribution, details of the surface SEM images of the 3D concentration-gradient Ni–Co hydroxide nanostructures at different deposition stages, CV and charge–discharge voltage curves of the counter Ketjenblack electrode, and photograph of a prototype of an asymmetric supercapacitor based on the 3D concentration-gradient Ni–Co hydroxide nanostructure lighting a green LED) is available in the online version of this article at http://dx.doi.org/10.1007/s12274-015-0781-3.

References

[1] Aricò, A. S.; Bruce, P.; Scrosati, B.; Tarascon, J. M.; Van Schalkwijk, W. Nanostructured materials for advanced energy conversion and storage devices. *Nat. Mater.* **2005**, *4*, 366–377.

[2] Huang, J. S.; Sumpter, B. G.; Meunier, V. Theoretical model for nanoporous carbon supercapacitors. *Angew. Chem. Int. Ed.* **2008**, *47*, 520–524.

[3] Chen, P. C.; Chen, H. T.; Qiu, J.; Zhou, C. W. Inkjet printing of single-walled carbon nanotube/RuO_2 nanowire supercapacitors on cloth fabrics and flexible substrates. *Nano Res.* **2010**, *3*, 594–603.

[4] Fang, M.; Tan, X. L.; Liu, M.; Kang, S. H.; Hu, X. Y.; Zhang, L. D. Low-temperature synthesis of Mn_3O_4 hollow–tetrakaidecahedrons and their application in electrochemical capacitors. *CrystEngComm* **2011**, *13*, 4915−4920.

[5] Selvan, R. K.; Perelshtein, I.; Perkas, N.; Gedanken, A. Synthesis of hexagonal–shaped SnO_2 nanocrystals and SnO_2@C nanocomposites for electrochemical redox supercapacitors. *J. Phys. Chem. C***2008**, *112*, 1825–1830.

[6] Wee, G.; Soh, H. Z.; Cheah, Y. L.; Mhaisalkar, S. G.; Srinivasan, M. Synthesis and electrochemical properties of electrospun V_2O_5 nanofibers as supercapacitor electrodes. *J. Mater. Chem.* **2010**, *20*, 6720–6725.

[7] Cheng, H.; Lu, Z.G.; Deng, J.Q.; Chung, C.Y.; Zhang, K. L.; Li, Y. Y. A facile method to improve the high rate capability of Co_3O_4 nanowire array electrodes. *Nano Res.* **2010**, *3*, 895–901.

[8] Lang, J. W.; Kong, L. B.; Wu, W. J.; Luo, Y. C.; Kang, L. Facile approach to prepare loose–packed NiO nano–flakes materials for supercapacitors. *Chem. Commun.* **2008**, *44*, 4213–4215.

[9] Zhu, J. W.; Chen, S.; Zhou, H.; Wang, X. Fabrication of a low defect density graphene–nickel hydroxide nanosheet hybrid with enhanced electrochemical performance. *Nano Res.* **2012**, *5*, 11–19.

[10] Du, H. M.; Jiao, L. F.; Wang, Q. H.; Yang, J. Q.; Guo, L. J.; Si, Y. C.; Wang, Y. J.; Yuan, H. T. Facile carbonaceous microsphere templated synthesis of Co_3O_4 hollow spheres and their electrochemical performance in supercapacitors. *Nano Res.* **2013**, *6*, 87–98.

[11] Mondal, C.; Ganguly, M.; Manna, P. K.; Yusuf, S. M.; Pal, T. Fabrication of porous β−$Co(OH)_2$ architecture at room temperature: A high performance supercapacitor. *Langmuir* **2013**, *29*, 9179–9187.

[12] Wang, H. L.; Holt, C. M. B.; Li, Z.; Tan, X. H.; Amirkhiz, B. S.; Xu, Z. W.; Olsen, B. C.; Stephenson, T.; Mitlin, D. Graphene–nickel cobaltite nanocomposite asymmetrical supercapacitor with commercial level mass loading. *Nano Res.* **2012**, *5*, 605–617.

[13] Xu, Y. X.; Huang, X. Q; Lin, Z.Y.; Zhong, X.; Huang, Y.; Duan, X. F. One–step strategy to graphene/$Ni(OH)_2$ composite hydrogels as advanced three-dimensional supercapacitor electrode materials. *Nano Res.* **2013**, *6*, 65–76.

[14] Lu, Z. Y.; Chang, Z.; Liu, J. F.; Sun, X. M. Stable ultrahigh specific capacitance of NiO nanorod arrays. *Nano Res.* **2011**, *4*, 658–665.

[15] Bao, L. H.; Li, X. D. Towards textile energy storage from cotton T-shirts. *Adv. Mater.* **2012**, *24*, 3246–3252.

[16] Huang, L.; Chen, D. C.; Ding, Y.; Feng, S.; Wang, Z. L.; Liu, M. L. Nickel–cobalt hydroxide nanosheets coated on

$NiCo_2O_4$ nanowires grown on carbon fiber paper for high-performance pseudocapacitors. *Nano Lett.* **2013**, *13*, 3135–3139.

[17] Yu, Z.Y.; Chen, L. F.; Yu, S. H. Growth of $NiFe_2O_4$ nanoparticles on carbon cloth for high performance flexible supercapacitors. *J. Mater. Chem. A* **2014**, *2*, 10889–10894.

[18] Wang, S. B.; Pu, J.; Tong, Y.; Cheng, Y. Y.; Gao, Y.; Wang, Z. H. $ZnCo_2O_4$ nanowire arrays grown on nickel foam for high-performance pseudocapacitors. *J. Mater. Chem. A* **2014**, *2*, 5434–5440.

[19] Yang, G. W.; Xu, C. L.; Li, H. L. Electrodeposited nickel hydroxide on nickel foam with ultrahigh capacitance. *Chem. Commun.* **2008**, *48,* 6537–6539.

[20] Wang, Y. M.; Zhao, D. D.; Zhao, Y. Q.; Xu, C. L.; Li, H. L. Effect of electrodeposition temperature on the electrochemical performance of a $Ni(OH)_2$ electrode. *RSC Adv.* **2012**, *2*, 1074–1082.

[21] Yang, G. W.; Xu, C. L.; Li, H. L. Electrodeposited nickel hydroxide on nickel foam with ultrahigh capacitance. *Chem. Commun.* **2008**, *44*, 6537–6539.

[22] Wang, H. L.; Holt, C. M. B.; Li, Z.; Tan, X. H.; Amirkhiz, B. S.; Xu, Z. W.; Olsen, B. C.; Stephenson, T.; Mitlin, D. Graphene-nickel cobaltite nanocomposite asymmetrical supercapacitor with commercial level mass loading. *Nano Res.* **2012**, *5*, 605–617.

[23] Li, J. X.; Yang, M.; Wei, J. P.; Zhou, Z. Preparation and electrochemical performances of doughnut−like $Ni(OH)_2$–$Co(OH)_2$ composites as pseudocapacitor materials. *Nanoscale* **2012**, *4*, 4498–4503.

[24] Lu, Z. Y.; Yang, Q.; Zhu, W.; Chang, Z.; Liu, J. F.; Sun, X. M.; Evans, D.; Duan, X. Hierarchical Co_3O_4@Ni-Co-O supercapacitor electrodes with ultrahigh specific capacitance per area. *Nano Res.* **2012**, *5*, 369–378.

[25] Gupta, V.;Gupta, S.; Miura, N. Potentiostatically deposited nanostructured Co_xNi_{1-x} layered double hydroxides as electrode materials for redox–supercapacitors. *J. Power Sources* **2008**, *175*, 680–685.

[26] Fan, Z. J.; Yan, J.; Wei, T.; Zhi, L. J.; Ning, G. Q.; Li, T. Y.; Wei, F. Asymmetric supercapacitors based on graphene/MnO_2 and activated carbon nanofiber electrodes with high power and energy density. *Adv. Funct. Mater.* **2011**, *21*, 2366–2375.

[27] Yu, G. H.; Hu, L. B.; Liu, N. A.; Wang, H. L.; Vosgueritchian, M.; Yang, Y.; Cui, Y.; Bao, Z. N. Enhancing the supercapacitor performance of graphene/MnO_2 nanostructured electrodes by conductive wrapping. *Nano Lett.* **2011**, *11*, 4438–4442.

[28] Pan, G. X.; Xia, X.; Cao, F.; Tang, P. S.; Chen, H. F. Porous $Co(OH)_2$/Ni composite nanoflake array for high performance supercapacitors. *Electrochim. Acta* **2012**, *63*, 335–340.

[29] Lee, J. W.; Ahn, T.; Soundararajan, D.; Ko, J. M.; Kim, J. D. Non-aqueous approach to the preparation of reduced graphene oxide/α-$Ni(OH)_2$ hybrid composites and their high capacitance behavior. *Chem. Commun.***2011**, *47*, 6305–6307.

[30] Ma, R.; Liang, J.; Takada, K.; Sasaki, T. Topochemical synthesis of Co–Fe layered double hydroxides at varied Fe/Co ratios: Unique intercalation of triiodide and its profound effect. *J. Am.Chem. Soc.* **2010**, *133*, 613–620.

[31] Liang, J. B.; Ma, R. Z.; Iyi, N.; Ebina, Y.; Takada, K.; Sasaki, T. Topochemical synthesis, anion exchange, and exfoliation of Co–Ni layered doublehydroxides: A route to positively charged Co–Ni hydroxide nanosheets with tunable composition. *Chem. Mater.* **2009**, *22*, 371–378.

[32] Wang, X.; Sumboja, A.; Lin, M. F.; Yan, J.; Lee, P. S. Enhancing electrochemical reaction sites in nickel–cobalt layered double hydroxides on zinc tin oxide nanowires: A hybrid material for an asymmetric supercapacitor device. *Nanoscale* **2012**, *4*, 7266–7272.